

Kitaev magnetism in honeycomb RuCl_3 with intermediate spin-orbit coupling

Heung-Sik Kim,¹ Vijay Shankar V.,¹ Andrei Catuneanu,¹ and Hae-Young Kee^{1,2,*}

¹*Department of Physics and Center for Quantum Materials, University of Toronto, 60 St. George St., Toronto, Ontario, M5S 1A7, Canada*
²*Canadian Institute for Advanced Research, Toronto, Ontario, M5G 1Z8, Canada*

Intensive studies of the interplay between spin-orbit coupling (SOC) and electronic correlations in transition metal compounds have recently been undertaken. In particular, $j_{\text{eff}} = 1/2$ bands on a honeycomb lattice provide a pathway to realize Kitaev's exactly solvable spin model. However, since current wisdom requires strong atomic SOC to make $j_{\text{eff}} = 1/2$ bands, studies have been limited to iridium oxides. Contrary to this expectation, we demonstrate how Kitaev interactions arise in $4d$ -orbital honeycomb $\alpha\text{-RuCl}_3$, despite having significantly weaker SOC than the iridium oxides, via assistance from electron correlations. A strong coupling spin model for these correlation-assisted $j_{\text{eff}} = 1/2$ bands is derived, in which large antiferromagnetic Kitaev interactions emerge along with ferromagnetic Heisenberg interactions. Our analyses suggest that the ground state is a zigzag-ordered phase lying close to the antiferromagnetic Kitaev spin liquid. Experimental implications for angle resolved photoemission spectroscopy, neutron scattering, and optical conductivities are discussed.

Introduction – Elucidating the cornucopia of novel physical phenomena exhibited by transition metal compounds with electrons occupying d orbitals has been a key focus of modern condensed matter physics. Relativistic effects such as spin-orbit coupling (SOC), which entangles the spin and orbital degrees of freedom, were largely ignored until recently when it was realized that these effects in cohort with electronic correlations could give rise to new ground states, including those with uncommon magnetic ordering.[1–8]

In particular, these effects bring about anisotropic exchange interactions that have been suggested as a way to engineer the exactly solvable Kitaev spin model[9] in the honeycomb iridate Na_2IrO_3 . These anisotropic interactions arise between two neighboring iridium (Ir) sites, each with a single $j_{\text{eff}} = 1/2$ state, through superexchange mediated by the p -orbitals on the intervening oxygen atoms that make up the edge-sharing octahedra around each Ir atom.[10, 11] This $j_{\text{eff}} = 1/2$ state, composed of an equal mixture of t_{2g} orbitals, which manifests at large SOC $\lambda \mathbf{L} \cdot \mathbf{S}$, where λ denotes the coupling strength, and \mathbf{S} and \mathbf{L} are spin and orbital angular momentum operators of the t_{2g} orbitals, respectively.

SOC is a relativistic effect roughly proportional to Z^4 , where Z is the atomic number, and hence studies so far have been limited to iridium ($Z=77$) and other heavy elements. Na_2IrO_3 and Li_2IrO_3 , while good candidates, suffer from trigonal lattice distortions and diminished two-dimensionality (2D) due to the Na atoms sandwiched between the honeycomb layers. The correct low-energy description is also under debate: single SOC-induced $j_{\text{eff}} = 1/2$ state versus nonrelativistic molecular orbitals.[12, 13] Thus, the search for more ideal 2D honeycomb materials described by a $j_{\text{eff}} = 1/2$ picture is important.

Recently, it was suggested that a ruthenium chloride $\alpha\text{-RuCl}_3$ (RuCl_3) is a good candidate because of its

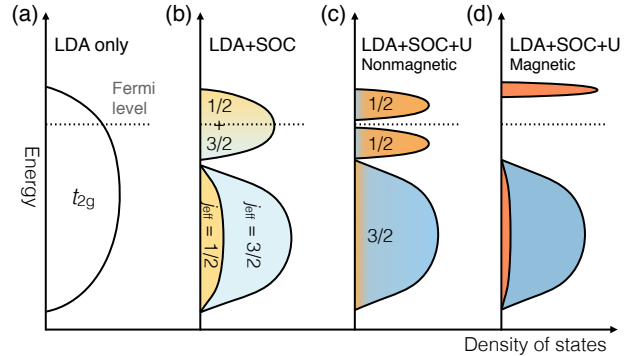


FIG. 1. (Color online) Schematic diagrams depicting the density of states (DOS) and change in the electronic structure of RuCl_3 as SOC and the on-site Coulomb interactions are included. Red and blue colors represent the weights of $j_{\text{eff}} = 1/2$ and $3/2$ states, respectively. Panel (a) displays the DOS without SOC, and panel (b) shows the DOS with SOC, which shows no clear separation between $j_{\text{eff}} = 1/2$ and $3/2$ bands. On including U and fixing a paramagnetic state, as shown in panel (c), the bands near the Fermi level acquire $j_{\text{eff}} = 1/2$ character and are separated from the $3/2$ bands. Panel (d) is the DOS in a magnetic ground state realized in RuCl_3 .

more ideal 2D honeycomb structure.[14] Although RuCl_3 should be metallic given the partially filled bands from the five valence electrons in t_{2g} orbitals, an insulating behavior is observed[15, 16], suggesting the possibility of a Mott insulating phase driven by electron correlations. A natural question follows about the role of SOC; naively one would expect that it would not play a major part as atomic SOC in Ru is $\lambda \sim 0.1$ eV[17], a fraction of that in Ir.

In this letter, we demonstrate that Kitaev magnetism can indeed be achieved in RuCl_3 despite its smaller atomic SOC strength. We arrive at this conclusion by first studying the role of electronic correlations using *ab-initio* electronic structure calculations. The results are

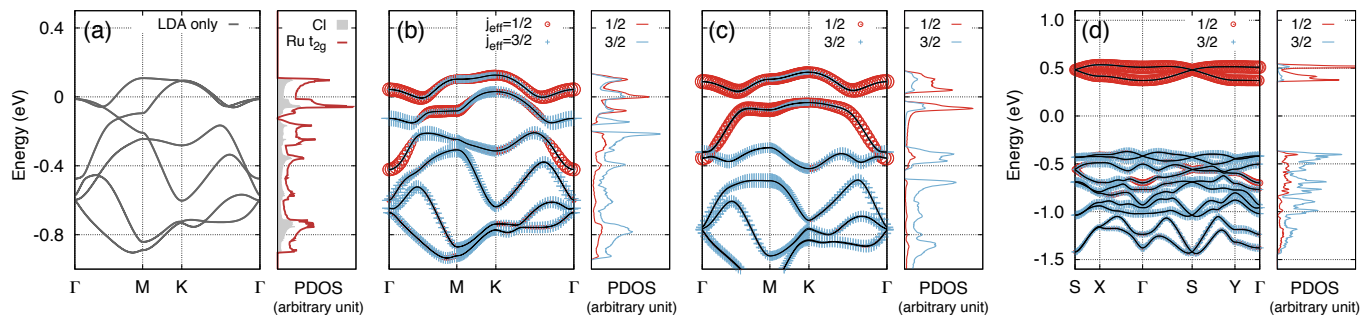


FIG. 2. (Color online) (a) Electronic structure of RuCl₃ without SOC and electron interactions. Red and gray curves depict the projected density of states (PDOS) for Cl, and Ru t_{2g} , respectively. The j_{eff} -projected band structures and density of states are laid out in the presence of SOC in (b), SOC and the on-site Coulomb interaction of $U_{\text{eff}} = 1.5$ eV while fixing a non-magnetic state in (c), and with the lowest energy zigzag (ZZ) magnetic order in (d), respectively.

summarized in the schematic density of states (DOS) depicted in Fig. 1. The t_{2g} bands without SOC are shown in Fig. 1(a). In the presence of SOC, the bands near the Fermi level are mixtures of $j_{\text{eff}} = 1/2$ and $3/2$ shown in Fig. 1(b). This mixing is quite a contrast to the band structure of iridates, where the $j_{\text{eff}} = 1/2$ and $3/2$ bands are well separated. Nevertheless, when the on-site Coulomb interaction U is introduced while fixing a paramagnetic state, the bands near the Fermi level take on a predominantly $j_{\text{eff}} = 1/2$ character and a band gap develops as shown in Fig. 1 (c), suggesting a correlation induced insulating phase. We further derive a spin Hamiltonian and determine spin exchange parameters in the strong SOC limit employing tight binding parameters obtained by projecting the *ab-initio* band structure. We find that zigzag (ZZ) magnetic order has the lowest energy, and its corresponding band structure is shown in Fig. 1 (d). We also discuss experimental tools to test our theory.

Ab-initio calculations – RuCl₃ has a layered honeycomb structure and a d^5 valence electron configuration for Ru³⁺, similar to the Ir⁴⁺ ion in Na₂IrO₃. While Na₂IrO₃ suffers from considerable lattice distortions, RuCl₃ has nearly perfect local cubic symmetry. Since the honeycomb layers of RuCl₃ are weakly coupled, we study a single honeycomb layer which should capture the important physics. We used OpenMX[18], which employs linear-combination-of-pseudo-atomic-orbitals, for the electronic structure calculations and confirmed our results with the Vienna Ab initio Simulation Package[19, 20]. Further details about our calculations are in the Supplementary Material[21].

The results of electronic structure calculations are presented in Fig. 2. Fig. 2(a) shows the bands and projected density of states (PDOS) of RuCl₃ without SOC and electronic interactions. The long Ru-Cl and Ru-Ru bonds result in a Ru t_{2g} bandwidth of only 1 eV, significantly smaller than the bandwidth of honeycomb iridates[12, 13, 22, 23]. The smaller bandwidth of RuCl₃

makes it more susceptible to SOC and correlations compared to its $5d$ counterparts. On the other hand, since each band in the t_{2g} manifold disperses across the entire bandwidth, the quasi-molecular orbital picture suggested for Na₂IrO₃ is unsuitable for RuCl₃[12]. Further clarification is provided in the supplementary material where the overlaps between the t_{2g} orbitals obtained by the maximally-localized Wannier orbital method[24] is described.

In the presence of SOC, the band structure and PDOS projected onto the j_{eff} states are shown in Fig. 2(b). The magnitude of Ru SOC is found to be 0.14 eV, which is small compared to the bandwidth. While one can distinguish the $j_{\text{eff}} = 1/2$ and $3/2$ bands near the Γ -point, they are mixed with each other near the Brillouin zone boundaries, especially near the K-point. PDOS shows that the j_{eff} -projected weights of the $1/2$ and $3/2$ states near the Fermi level are comparable, showing that unlike its $5d$ counterpart Na₂IrO₃, SOC alone is insufficient to support the $j_{\text{eff}} = 1/2$ picture in RuCl₃. The on-site Coulomb interactions in Ru d -orbitals, however, does promote the $j_{\text{eff}} = 1/2$ picture.

We performed LDA+SOC+ U calculations fixing a paramagnetic (PM) phase to understand the combined effects of interactions and SOC without a magnetic order. Fig. 2(c) shows the PM results with $U_{\text{eff}} \equiv U - J_{\text{H}} = 1.5$ eV (J_{H} is Hund's coupling), which is a metastable solution that can be obtained by slowly increasing U_{eff} from the noninteracting starting point. Compared to Fig. 2(b), one can see that the $j_{\text{eff}} = 3/2$ states are pushed down significantly, so that the low-energy states near the Fermi level can be described purely in terms of the $j_{\text{eff}} = 1/2$ states. The effective SOC at $U_{\text{eff}} = 1.5$ eV is about twice the atomic value, a dramatic enhancement compared to results reported for iridates recently[25]. Previously, such an enhancement was reported for the $4d$ transition metal oxide Sr₂RhO₄. [26]

Having established how correlations lead to a $j_{\text{eff}} = 1/2$ picture in RuCl₃, we studied the energies of five differ-

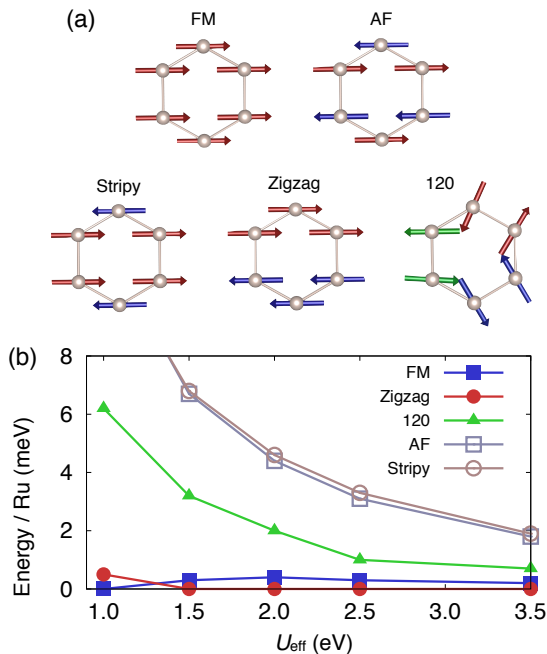


FIG. 3. (Color online) (a) Collinear magnetic configurations considered in the LDA+SOC+ U calculations. (b) Relative energy difference per Ru atom for each configuration plotted with respect to U_{eff} . The ZZ ordered state has the lowest energy except when $U_{\text{eff}} = 1.0\text{eV}$, but FM is competitive and the 120 ordered state approaches both states in energy when U_{eff} is large.

ent magnetic phases shown in Fig. 3 (a) – ferromagnet (FM), antiferromagnet (AF), stripy (ST), zigzag (ZZ), and 120 order. The relative energy differences between these phases as a function of U_{eff} is shown in Fig. 3 (b). We find that the ZZ phase is the ground state over the entire range of U_{eff} up to 3.5 eV, except at $U_{\text{eff}} = 1.0\text{eV}$ where the FM phase has lower energy. In the higher U_{eff} regime, ZZ is nearly degenerate with FM and 120 ordering. The electronic band structure for this ZZ state is shown in Fig. 2(d). After the magnetic order sets in, the $j_{\text{eff}} = 1/2$ bands are further pushed away (the gap increases), and the occupied $j_{\text{eff}}=1/2$ band is now mixed with the $j_{\text{eff}} = 3/2$ bands.

$j_{\text{eff}}=1/2$ spin model in the strong coupling limit – As RuCl_3 is considered a Mott insulator[14], we construct a strong coupling spin model to capture the possible magnetic phases of RuCl_3 . Our analysis of correlation enhanced SOC allows us to construct a spin model based on pseudospin $j_{\text{eff}}=1/2$ states near the Fermi level. On each bond we fix a spin direction γ and label the bond $\alpha\beta(\gamma)$ as in Fig.4(a), with α and β being the remaining two spin directions. The spin Hamiltonian relevant for

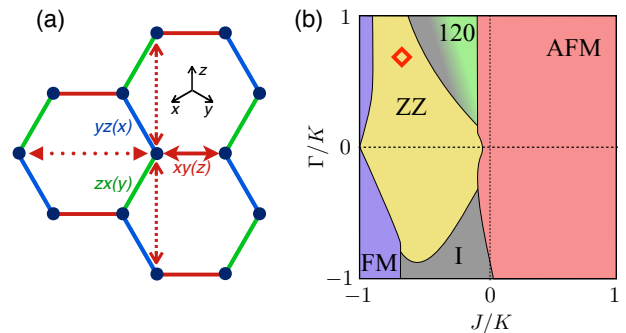


FIG. 4. (Color online) (a) 1st (solid), 2nd (dashed), and 3rd (dotted) n.n bonds on the honeycomb lattice with the bond labels. Red, blue, and green colors depict the $\alpha\beta(\gamma) = xy(z)$, $yz(x)$, and $zx(y)$ bond, respectively, where α , β , and γ denote the spin components interacting on the specified bond. Further neighbor hoppings with only $xy(z)$ -type are depicted in the figure. (b) shows the Luttinger-Tisza phase diagram at $J_{\text{H}}/U = 0.2$ for fixed 2nd and 3rd n.n exchanges. Grey shading within the 120 order phase depicts the trace of incommensurate (I) order occurring in that area. The red diamond marks the estimated parameters for RuCl_3 . See the main text for a description of the exchange parameters.

RuCl_3 , obtained from *ab-initio* results is then,

$$\begin{aligned}
 H = & \sum_{\langle ij \rangle \in \alpha\beta(\gamma)} \left(J \mathbf{S}_i \cdot \mathbf{S}_j + K S_i^\alpha S_j^\alpha + \Gamma (S_i^\alpha S_j^\beta + S_i^\beta S_j^\alpha) \right) \\
 & + \sum_{\langle\langle ij \rangle\rangle \in \alpha\beta(\gamma)} \left(J_2^\alpha S_i^\alpha S_j^\alpha + J_2^\beta S_i^\beta S_j^\beta + J_2^\gamma S_i^\gamma S_j^\gamma \right) \\
 & + \sum_{\langle\langle\langle ij \rangle\rangle\rangle \in \alpha\beta(\gamma)} \left(J_3 \mathbf{S}_i \cdot \mathbf{S}_j + K_3 S_i^\alpha S_j^\alpha + \Gamma_3 (S_i^\alpha S_j^\beta + S_i^\beta S_j^\alpha) \right),
 \end{aligned} \quad (1)$$

where i, j label the Ru^{3+} sites and \mathbf{S}_i is a $j_{\text{eff}}=1/2$ spin operator with components S_i^α . The parameters J and K are Heisenberg and Kitaev exchanges respectively, and Γ is a symmetric off-diagonal exchange. $J_2^{(x,y,z)}$ are anisotropic spin exchanges at the 2nd n.n level while J_3 , K_3 and Γ_3 are the 3rd n.n analogues to the n.n exchanges.

Since the exchanges are expressed in terms of overlaps between t_{2g} states, the on-site Coulomb interaction U , and the Hund's coupling J_{H} , they can be estimated using the tight-binding parameters deduced from the *ab-initio* calculations. For fixed $J_{\text{H}}/U = 0.2$, we find that the n.n terms dominate with antiferromagnetic K , ferromagnetic J , and positive Γ . Including n.n t_{2g} - e_g exchange processes in addition to the ones within t_{2g} , we estimate the n.n exchanges to be $J/K \simeq -0.7$ and $\Gamma/K \simeq 0.7$. The estimates for the 2nd n.n exchanges on a z -bond denoted by red dashed lines in Fig.4 are $J_2^x/K \simeq -0.03$, $J_2^y/K \simeq -0.01$, $J_2^z/K \simeq -0.01$ and those for 3rd n.n are $J_3/K \simeq 0.02$, $K_3/K \simeq 0.03$ with vanishingly small Γ_3/K . We note that the Kitaev exchange is further enhanced due to inter-orbital t_{2g} - e_g hopping.[27] For more details, including explicit expressions for the exchanges

and tight-binding parameters, see the Supplementary Material.

Luttinger-Tisza analyses[28] were performed to obtain classical ground states of the above model. A phase diagram for varying J/K and Γ/K while keeping $J_2^{(x,y,z)}/K$, J_3/K , and K_3/K fixed is presented in Fig. 4(b). Based on the strength of the exchanges (see Supplementary Material) we find that the relevant position for RuCl_3 , denoted by a red diamond in Fig. 4(b), is in the ZZ regime close to FM and 120 ordered states. While the qualitative features of the phase diagram are well captured by the n.n J - K - Γ model, addition of 2nd and 3rd n.n exchanges enlarges the ZZ region. This enhancement of the ZZ phase on adding further neighbor exchanges was also observed for $J_H/U = 0.3$ and is likely independent of the J_H/U ratio. Our analysis predicts that RuCl_3 has a zigzag ordered ground state, described by a pseudospin $j_{\text{eff}}=1/2$ model, lying close to the antiferromagnetic Kitaev spin liquid. It is remarkable that the ZZ phase is surrounded by FM and 120 ordered phases in the strong-coupling phase diagram, these states are also found to be very close in energy in our LDA+SOC+ U calculations.

Discussion and Conclusion – There are various experimental ways to test our proposal. One experimental technique is angle resolved photoemission spectroscopy (ARPES), which is ideal for RuCl_3 with its layered structure. Occupied states below the Fermi level should reflect a large gap as well as flat dispersion across the Brillouin zone.

In the iridates, the first measurement that stimulated the idea of Sr_2IrO_4 being a spin-orbit Mott insulator was the optical conductivity, where an optical gap of around 0.5 eV was seen[29]. In RuCl_3 however, previous optical data was interpreted in terms of a small optical gap of 0.2 - 0.3 eV, but the extremely small intensity in this region suggests that this feature may not be associated with charge excitations[30]. Provided the optical gap is identified with the onset of the peak at around 1eV in existing studies[14, 15, 31], which is bigger than the observed values of 0.5 eV in Sr_2IrO_4 [29] and 0.34 eV in Na_2IrO_3 [32], our results are in good agreement with the optical data.

Our prediction of ZZ magnetic order in the ground state, should be detectable by neutron scattering. An elastic neutron scattering measurement that has just been reported found a magnetic peak at the wave-vector \mathbf{M} below 8 K[33], suggesting that the magnetic order is either ZZ or ST. Based on the analysis of anisotropy in susceptibility provided in Ref. 33 and 34, we find an antiferromagnetic K , a ferromagnetic J which is a fraction of K , and a finite Γ . Thus, ZZ magnetic order should be consistent with both neutron and susceptibility data. Inelastic neutron scattering analysis, similar to the one reported for Na_2IrO_3 [35], can provide further confirmation, since the spin-wave spectra including spin gaps are different in the ZZ and ST phases. Thus computing spin

wave excitations in various regimes of the strong-coupling model would be a natural step for a future study.

It is important to note that although RuCl_3 shows a ZZ ordered phase similar to Na_2IrO_3 , the microscopic origins of the two ZZ ordered phases are quite different. The Kitaev interaction is antiferromagnetic in RuCl_3 , while it is ferromagnetic in Na_2IrO_3 . This is because the Kitaev exchange originates from oxygen mediated hopping in Na_2IrO_3 , while in RuCl_3 , it is primarily due to direct overlap of d orbitals. The difference between the two compounds comes from the difference of covalency between oxygen and chlorine ions, suggesting that qualitative features of the underlying low-energy physics depends on structural and chemical details in these layered honeycomb compounds. The different magnetic ground states in Na_2IrO_3 and Li_2IrO_3 which shows an incommensurate spiral magnetic order[36] is another example. In this regard, a comparative study of RuCl_3 and Li_2RhO_3 , which is isostructural and isoelectronic to Li_2IrO_3 [37], can be interesting as both share similar SOC strengths and electron correlations but have different lattice constants and p -orbital covalency.

In summary, combining *ab-initio* and strong coupling approaches, we have investigated the electronic and magnetic properties of RuCl_3 . Our results strongly suggest that this compound can be understood as an interaction-driven $j_{\text{eff}} = 1/2$ system, which hosts magnetism dominated by the Kitaev interaction. Owing to the simple and ideal crystal structure, RuCl_3 provides an excellent platform to explore the physics of SOC and electronic correlations as well as related unconventional magnetism. Our study also opens up the possibility of a whole new class of materials in which to explore physics driven by spin-orbit coupling and electronic correlations, beyond the 5d transition metal oxides.

Acknowledgements – We thank Y.-J. Kim, K.S. Burch, L. Sandilands, and E.K.-H Lee for useful discussions and R. Schaffer for a critical reading of the manuscript. This work was supported by the NSERC of Canada and the center for Quantum Materials at the University of Toronto. Computations were mainly performed on the GPC supercomputer at the SciNet HPC Consortium. SciNet is funded by: The Canada Foundation for Innovation under the auspices of Compute Canada; the Government of Ontario; Ontario Research Fund for Research Excellence; and the University of Toronto. HSK thanks the IBS Center for Correlated Electron System at Seoul National University for additional computational resources and V.S.V thanks NSERC-CREATE for a graduate fellowship through the HEATER program.

* hykee@physics.utoronto.ca

[1] W. Witczak-Krempa, G. Chen, Y. B. Kim, and L. Ba-

- lents, *Annu. Rev. Condens. Matter Phys.* **5**, 57 (2014).
- [2] X. Wan, A. M. Turner, A. Vishwanath, and S. Y. Savrasov, *Phys. Rev. B* **83**, 205101 (2011).
- [3] E.-G. Moon, C. Xu, Y. B. Kim, and L. Balents, *Phys. Rev. Lett.* **111**, 206401 (2013).
- [4] J. Maciejko, V. Chua, and G. A. Fiete, *Phys. Rev. Lett.* **112**, 016404 (2014).
- [5] D. Pesin and L. Balents, *Nature Physics* **6**, 376 (2010).
- [6] M. J. Lawler, H.-Y. Kee, Y. B. Kim, and A. Vishwanath, *Phys. Rev. Lett.* **100**, 227201 (2008).
- [7] Y. Chen and H.-Y. Kee, *Phys. Rev. B* **90**, 195145 (2014).
- [8] Y. Chen, Y.-M. Lu, and H.-Y. Kee, *Nat. Commun.* **6**, 6593 (2015).
- [9] A. Kitaev, *Ann. Phys.* **321**, 2 (2006).
- [10] G. Khaliullin, *Prog. Theor. Phys. Supp.* **160**, 155 (2005).
- [11] G. Jackeli and G. Khaliullin, *Phys. Rev. Lett.* **102**, 017205 (2009).
- [12] I. I. Mazin, H. O. Jeschke, K. Foyevtsova, R. Valentí, and D. I. Khomskii, *Phys. Rev. Lett.* **109**, 197201 (2012).
- [13] H.-S. Kim, C. H. Kim, H. Jeong, H. Jin, and J. Yu, *Phys. Rev. B* **87**, 165117 (2013).
- [14] K. Plumb, J. Clancy, L. Sandilands, V. Vijay Shankar, Y. Hu, K. Burch, H.-Y. Kee, and Y.-J. Kim, *Phys. Rev. B* **90**, 041112 (2014).
- [15] L. Binotto, I. Pollini, and G. Spinolo, *Phys. Status Solidi (b)* **44**, 245 (1971).
- [16] I. Pollini, *Phys. Rev. B* **53**, 12769 (1996).
- [17] W. W. Porterfield, *Inorganic Chemistry* (Academic press, 2013).
- [18] T. Ozaki, *Phys. Rev. B* **67**, 155108 (2003); <http://www.openmx-square.org>.
- [19] G. Kresse and J. Hafner, *Phys. Rev. B* **47**, 558 (1993).
- [20] G. Kresse and J. Furthmüller, *Phys. Rev. B* **54**, 11169 (1996).
- [21] See Supplemental Material for computational details and further information on tight-binding parameters and exchange interactions.
- [22] K. Foyevtsova, H. O. Jeschke, I. Mazin, D. Khomskii, and R. Valentí, *Phys. Rev. B* **88**, 035107 (2013).
- [23] C. H. Kim, H. S. Kim, H. Jeong, H. Jin, and J. Yu, *Phys. Rev. Lett.* **108**, 106401 (2012).
- [24] N. Marzari and D. Vanderbilt, *Phys. Rev. B* **56**, 12847 (1997).
- [25] H.-S. Kim, Y. Chen, and H.-Y. Kee, *Phys. Rev. B* **91**, 235103 (2015).
- [26] G.-Q. Liu, V. N. Antonov, O. Jepsen, and O. K. Andersen, *Phys. Rev. Lett.* **101**, 026408 (2008).
- [27] J. Chaloupka, G. Jackeli, and G. Khaliullin, *Phys. Rev. Lett.* **110**, 097204 (2013).
- [28] J. M. Luttinger and L. Tisza, *Phys. Rev.* **70**, 954 (1946).
- [29] B. Kim, H. Jin, S. Moon, J.-Y. Kim, B.-G. Park, C. Leem, J. Yu, T. Noh, C. Kim, S.-J. Oh, *et al.*, *Phys. Rev. Lett.* **101**, 076402 (2008).
- [30] L. J. Sandilands, Y. Tian, A. A. Reijnders, H.-S. Kim, K. W. Plumb, H.-Y. Kee, Y.-J. Kim, and K. S. Burch, *arXiv preprint*, arXiv:1503.07593 (2015).
- [31] G. Guizzetti, E. Reguzzoni, and I. Pollini, *Phys. Lett.* **70A**, 34 (1979).
- [32] R. Comin, G. Levy, B. Ludbrook, Z.-H. Zhu, C. Veenstra, J. Rosen, Y. Singh, P. Gegenwart, D. Stricker, J. N. Hancock, *et al.*, *Phys. Rev. Lett.* **109**, 266406 (2012).
- [33] J. A. Sears, M. Songvilay, K. W. Plumb, J. P. Clancy, Y. Qiu, Y. Zhao, D. Parshall, and Y.-J. Kim, *Phys. Rev. B* **91**, 144420 (2015).
- [34] J. G. Rau, E. K.-H. Lee, and H.-Y. Kee, *Phys. Rev. Lett.* **112**, 077204 (2014).
- [35] S. K. Choi, R. Coldea, A. N. Kolmogorov, T. Lancaster, I. I. Mazin, S. J. Blundell, P. G. Radaelli, Y. Singh, P. Gegenwart, K. R. Choi, S.-W. Cheong, P. J. Baker, C. Stock, and J. Taylor, *Phys. Rev. Lett.* **108**, 127204 (2012).
- [36] Y. Singh, S. Manni, J. Reuther, T. Berlijn, R. Thomale, W. Ku, S. Trebst, and P. Gegenwart, *Phys. Rev. Lett.* **108**, 127203 (2012).
- [37] I. I. Mazin, S. Manni, K. Foyevtsova, H. O. Jeschke, P. Gegenwart, and R. Valentí, *Phys. Rev. B* **88**, 035115 (2013).
- [38] J. Chaloupka, G. Jackeli, and G. Khaliullin, *Phys. Rev. Lett.* **110**, 097204 (2013).
- [39] H. Weng, T. Ozaki, and K. Terakura, *Phys. Rev. B* **79**, 235118 (2009).
- [40] H.-S. Kim, E. K.-H. Lee, and Y. B. Kim, *arXiv preprint* arXiv:1502.00006 (2015).
- [41] J. Reuther, R. Thomale, and S. Rachel, *Phys. Rev. B* **90**, 100405 (2014).
- [42] Among the four processes mentioned in Ref. [38] — i) σ -type direct hopping, ii) t_{2g} - e_g process, iii) d - p - d indirect process, and iv) p - d charge transfer excitation —, i) and iii) are already taken into account in our results, and iv) should be less significant compared to the other three contributions due to the weaker hybridization between the Ru t_{2g} and Cl p orbitals as shown in Fig. 2(a) in the main text.
- [43] J. P. Perdew and A. Zunger, *Phys. Rev. B* **23**, 5048 (1981).
- [44] M. J. Han, T. Ozaki, and J. Yu, *Phys. Rev. B* **73**, 045110 (2006).
- [45] S. L. Dudarev, G. A. Botton, S. Y. Savrasov, C. J. Humphreys, and A. P. Sutton, *Phys. Rev. B* **57**, 1505 (1998).
- [46] A. I. Liechtenstein, V. I. Anisimov, and J. Zaanen, *Phys. Rev. B* **52**, R5467 (1995).

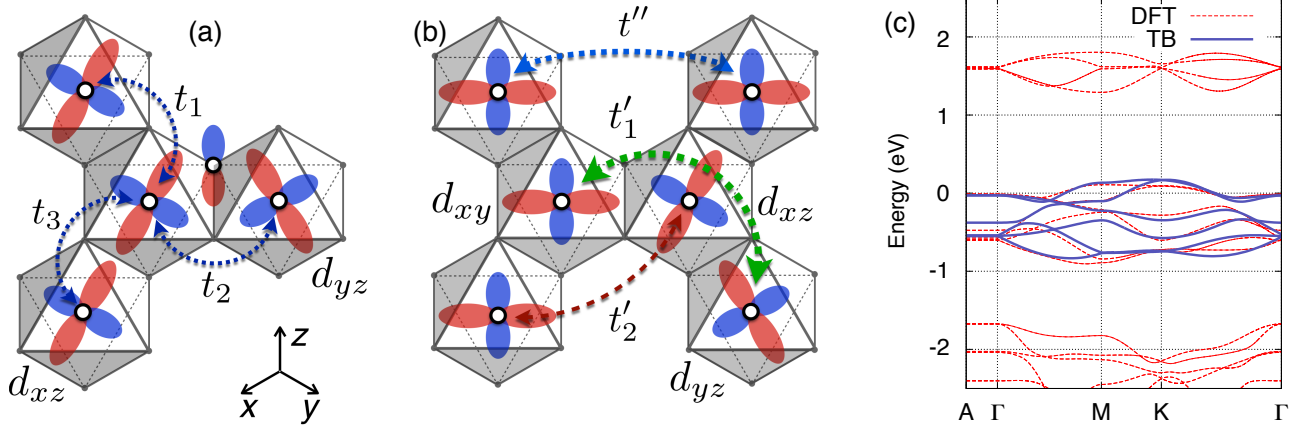


FIG. S1. (Color online) (a-b) Six major hopping channels between neighboring Ru t_{2g} orbitals, where (a) shows the nearest-neighbor (n.n) and (b) shows second (2nd) and third (3rd) n.n overlaps. (c) Band structure of RuCl₃ monolayer, where dashed red lines show *ab-initio* bands without SOC and on-site Coulomb interactions, and the tight-binding (TB) bands from the overlaps depicted in (a) and (b) are in solid blue.

SUPPLEMENTARY MATERIAL A: DETAILS ON t_{2g} OVERLAPS

In order to understand the hopping processes between Ru t_{2g} orbitals better and for estimating the exchange interactions, we calculated the overlaps using maximally-localized Wannier orbital calculations without and with the presence of SOC[24, 39]. Due to the virtually ideal crystal structure and large distances between Ru atoms, six major hoppings suffice to reproduce the electronic structure. Since the inclusion of SOC induce only small change (less than 2 meV) to the hopping terms except the on-site SOC terms, here we show the results from non-relativistic calculations. Fig. S1(a) shows the three nearest neighbor (n.n) hoppings; t_1 , t_2 , and t_3 , where t_1 and t_3 are intra-orbital overlaps where as t_2 is an inter-orbital overlap. The largest overlap, t_3 , is dominated by the σ -type direct overlap between Ru t_{2g} orbitals, while t_2 has contributions from π -type direct overlap in addition to indirect d - p - d contribution via the p -orbitals of intervening Chlorine atoms. t_1 is due to π - and δ -type direct overlap. Small distortions in the crystal structure give rise to anisotropies less than 5 meV in the hoppings so we take their average to obtain $t_1 = 65$ meV, $t_2 = 113$ meV, and $t_3 = -226$ meV. In the second (2nd) n.n hopping channels, depicted in Fig. S1(b), there are two inequivalent inter-orbital hoppings t'_1 and t'_2 due to the absence of inversion symmetry with respect to the bond center. In t'_1 channel the orbital lobes participating in the hopping point towards the intermediate Ir site, while in t'_2 they are directed towards the center of the honeycomb. There are also third (3rd) n.n intra-orbital hoppings denoted by t'' . Their magnitudes are $t'_1 = -20$ meV, $t'_2 = -58$ meV, and $t'' = -49$ meV, and have no direction dependence unlike in the case of n.n hopping channels.

All other overlaps are less than 10 meV and can be considered marginal; tight-binding band structure from the six major contributions shows good agreement with the *ab-initio* bands in Fig. S1(c). Note that unlike in several two- and three-dimensional honeycomb iridates where t_2 is dominant[13, 22, 40], in RuCl₃ t_3 is twice as large as t_2 . The quasimolecular orbital character in the two-dimensional iridate Na₂IrO₃[12] originates from this t_2 overlap. Since it is not the principal overlap in RuCl₃, the conventional t_{2g} orbital picture is more appropriate for understanding the electronic structure. Detailed hopping magnitudes are provided in Table I.

\mathbf{T}_{ij}	n.n			2nd n.n			3rd n.n		
	$\mathbf{r}_{ij} = (-d, +d, 0)$			$\mathbf{r}_{ij} = (-d, -d, +2d)$			$\mathbf{r}_{ij} = (-2d, +2d, 0)$		
	$A \rightarrow B$			$A \rightarrow A$			$B \rightarrow A$		
	d_{xy}	d_{yz}	d_{xz}	d_{xy}	d_{yz}	d_{xz}	d_{xy}	d_{yz}	d_{xz}
d_{xy}	-0.229	-0.010	-0.011	0.000	+0.006	+0.004	-0.049	+0.009	+0.009
d_{yz}	-0.011	+0.065	+0.114	+0.003	0.000	-0.020	+0.010	-0.008	-0.005
d_{xz}	-0.009	+0.113	+0.066	+0.006	-0.058	0.000	+0.009	-0.005	-0.008

TABLE I. (Unit in eV) A subset of Ru t_{2g} hoppings \mathbf{T}_{ij} as representatives of each hopping channel up to third NN, where $H_{t_{2g}} = \sum_{ij} \mathbf{C}_i^\dagger \cdot \mathbf{T}_{ij} \cdot \mathbf{C}_j$ with \mathbf{C}^\dagger and \mathbf{C} being the creation and annihilation operators for t_{2g} states, respectively. A and B are sublattice indices, and \mathbf{r}_{ij} is expressed in terms of the coordinates depicted in Fig. S1(a-b), where $d \simeq 2.43\text{\AA}$ is approximate distance between Ru and Cl. Other hoppings can be recovered by applying $\mathbf{T}_{ji} = \mathbf{T}_{ij}^\dagger$, $\mathbf{T}_{A \rightarrow A} = (\mathbf{T}_{B \rightarrow B})^\dagger$, C_3 rotations along the threefold axis perpendicular to the honeycomb plane, and inversion operations.

SUPPLEMENTARY MATERIAL B: EXCHANGE INTERACTIONS

The pseudospin $j_{\text{eff}} = 1/2$ spin Hamiltonian (Eq.1 in the main text) is,

$$\begin{aligned}
H = & \sum_{\langle ij \rangle \in \alpha\beta(\gamma)} \left(J\mathbf{S}_i \cdot \mathbf{S}_j + K S_i^\gamma S_j^\gamma + \Gamma (S_i^\alpha S_j^\beta + S_i^\beta S_j^\alpha) \right) \\
& + \sum_{\langle\langle ij \rangle\rangle \in \alpha\beta(\gamma)} \left(J_2^\alpha S_i^\alpha S_j^\alpha + J_2^\beta S_i^\beta S_j^\beta + J_2^\gamma S_i^\gamma S_j^\gamma \right) \\
& + \sum_{\langle\langle\langle ij \rangle\rangle\rangle \in \alpha\beta(\gamma)} \left(J_3\mathbf{S}_i \cdot \mathbf{S}_j + K_3 S_i^\gamma S_j^\gamma + \Gamma_3 (S_i^\alpha S_j^\beta + S_i^\beta S_j^\alpha) \right).
\end{aligned}$$

Explicit expressions of the exchange interactions for the n.n $j_{\text{eff}}=1/2$ spins derived in Ref. 34 are:

$$\begin{aligned}
J &= \frac{4}{27} \left[\frac{6t_1(t_1 + 2t_3)}{U - 3J_H} + \frac{2(t_1 - t_3)^2}{U - J_H} + \frac{(2t_1 + t_3)^2}{U + 2J_H} \right] \\
K &= \frac{8J_H}{9} \left[\frac{(t_1 - t_3)^2 - 3t_2^2}{(U - 3J_H)(U - J_H)} \right] \\
\Gamma &= \frac{16J_H}{9} \left[\frac{t_2(t_1 - t_3)}{(U - 3J_H)(U - J_H)} \right].
\end{aligned} \tag{S1}$$

For the 2nd n.n interactions, due to the asymmetry of the hopping channels at the three J_2^α ($\alpha = x, y, z$) exchanges are different. In terms of t'_1, t'_2, U and J_H they can be written as below:

$$\begin{aligned}
J_2^x &= -\frac{4U}{9} \frac{(t'_1 - t'_2)^2}{(U + 2J_H)(U - 3J_H)} + \frac{4J_H}{9} \frac{(t'_2 - t'_1)^2}{(U - J_H)(U - 3J_H)(U + 2J_H)} \simeq -J_2^0 + \frac{8}{9U} t' (t' - t'_p) \left(\frac{J_H}{U} \right), \\
J_2^y &= -\frac{4U}{9} \frac{(t'_1 - t'_2)^2}{(U + 2J_H)(U - 3J_H)} - \frac{4J_H}{9} \frac{(t'_2 - t'_1)^2}{(U - J_H)(U - 3J_H)(U + 2J_H)} \simeq -J_2^0 + \frac{8}{9U} t'_p (t'_p - t') \left(\frac{J_H}{U} \right), \\
J_2^z &= +\frac{4U}{9} \frac{(t'_1 - t'_2)^2}{(U + 2J_H)(U - 3J_H)} - \frac{4J_H}{9} \frac{(t'_1 + t'_2)^2 + 2t'_1 t'_2}{(U - J_H)(U - 3J_H)(U + 2J_H)} \simeq +J_2^0 - \frac{8}{9U} (t' + t'_p)^2 \left(\frac{J_H}{U} \right),
\end{aligned} \tag{S2}$$

for the $xy(z)$ bond, where $J_2^0 = 4 \frac{(t'_1 - t'_2)^2}{9U}$. Note that, when the Hund's coupling becomes small, the 2nd n.n interactions reduce to ferromagnetic Heisenberg ($\simeq -J_2^0$) and antiferromagnetic Kitaev ($\simeq 2J_2^0$) interactions with the Kitaev exchange having twice the magnitude of the Heisenberg exchange. Similar 2nd n.n exchanges have also been observed for other layered honeycomb iridates [13, 41]. Lastly, the expression for the 3rd n.n exchange interactions are obtained by substituting t_3 to t'' and setting t_1 and t_2 to be zero in Eq. (1).

Additional superexchange process through the e_g -excited states is possible and can be non-negligible due to the small energy splitting of $\Delta E_{e_g - t_{2g}} \sim 1.5$ eV between them as shown in Fig. S1(c). In Ref. 38 it was suggested that, this t_{2g} - e_g process can give rise to ferromagnetic Heisenberg and antiferromagnetic Kitaev interactions [42]. Owing to the nearly distortion-free structure of RuCl_3 , only one hopping channel is active in this process; d_{xy} -to- $d_{3z^2-r^2}$

hopping along the horizontal “z-bond” in Fig. S1(a) and (b). The expression is, as shown in Ref. 38, as follows;

$$\begin{aligned}
 H' &= \sum_{\langle ij \rangle \in \gamma} I' (2S_i^\gamma S_j^\gamma - \mathbf{S}_i \cdot \mathbf{S}_j) \\
 I' &\simeq \frac{4}{9\tilde{U}} \tilde{t}^2 \left(\frac{\tilde{J}_H}{\tilde{U}} \right),
 \end{aligned} \tag{S3}$$

where $\tilde{J}_H \sim J_H$ and \tilde{U} are the Hund’s coupling and the effective excitation energy between the t_{2g} and e_g states, and $\tilde{t} = 190$ meV is the t_{2g} - e_g overlap obtained from the Wannier orbital calculations. The two processes — intra- t_{2g} and t_{2g} - e_g processes — have the same direction dependence, and both the Kitaev interactions add up to yield a larger one. Using $J_H/U = 0.2$, $U \approx 3$ eV and $\tilde{U} \approx 1.5$ eV, we get the ratios $J/K \simeq -0.7$ and $\Gamma/K \simeq 0.7$, $J_2^x/K \simeq -0.03$, $J_2^y/K \simeq -0.01$, $J_2^z/K \simeq -0.01$, $J_3/K \simeq 0.02$, $K_3/K \simeq 0.03$, and vanishingly small Γ_3/K as presented in the main text.

SUPPLEMENTARY MATERIAL C: COMPUTATIONAL DETAILS

For the electronic structure calculations with SOC and on-site Coulomb interactions, OPENMX [18], which is based on the linear-combination-of-pseudo-atomic-orbitals, is used. A non-collinear DFT scheme and a fully relativistic j -dependent pseudopotential are used to treat SOC, with the Perdew-Zunger parametrization of the local density approximation (LDA) chosen for the exchange-correlation functional[43]. 500 Ry of energy cutoff was used for the real-space sampling, and $8 \times 8 \times 1$ k -grid was adopted for the primitive cell. On-site Coulomb interactions are treated via a simplified LDA+ U formalism implemented in OPENMX code[44, 45], with up to 3.5 eV of $U_{\text{eff}} \equiv U - J_H$ parameter used for Ru d -orbitals in our LDA+SOC+ U calculations. Maximally-localized Wannier orbitals method[24] implemented in OPENMX [39], is used to obtain the tight-binding Hamiltonian for Ru t_{2g} and e_g orbitals.

The LDA+SOC+ U results for the paramagnetic phase was doubled-checked using Vienna Ab-initio Simulation Package[19, 20]. To check the effect of J_H on our results, Liechtenstein’s more general LDA+ U formalism was employed, which treats the role of J_H explicitly[46]. A plane-wave energy cutoff of 400 eV and $13 \times 13 \times 1$ k-points for the k-point sampling were used. Using $U = 2.0$ eV and $J_H = 0.4$ eV, equivalent to $U_{\text{eff}} = 1.6$ eV, yields same results with OPENMX calculations; effective SOC is enhanced.